A Diagnostic Comparison of Alaskan and Siberian Strong Anticyclones

JUSTIN E. JONES AND JUDAH COHEN

Atmospheric and Environmental Research, Inc., Lexington, Massachusetts

Journal of Climate

(revised)

8 November 2010

Corresponding author address: Justin E. Jones, Atmospheric and Environmental Research, Inc., 131 Hartwell Ave., Lexington, MA 02421. Email: jjones@aer.com

ABSTRACT

Strong anticyclones have a significant impact on the cool season climate over mid- and high-latitude landmasses as they are typically accompanied by arctic air masses that can eventually move into populated mid-latitude regions. Composite analyses of Alaskan and Siberian strong anticyclones based on sea level pressure (SLP) thresholds of 1050 and 1060 hPa, respectively, were performed to diagnose large-scale dynamical and thermodynamical parameters associated with the formation of strong anticyclones over these two climatologically favorable regions. The anticyclone composite analyses indicate the presence of moderate to high amplitude ridge-trough patterns associated with anticyclogenesis. These ridge-trough patterns are critical as they lead to dynamically favorable circumstances for rapid anticyclogenesis.

The strong Alaskan anticyclone develops downstream of a highly amplified 300-hPa ridge and is associated with a region of strong tropospheric subsidence due to differential anticyclonic vorticity advection and cold-air advection over the anticyclone center. The strong Siberian anticyclone is associated with a 300-hPa pattern of lesser amplitude, suggesting that these dynamical factors, while still important, are less critical to its development. The relative location of elevated terrain features also appears to contribute greatly to the overall evolution of each of these anticyclones.

1. Introduction

Strong polar anticyclones are a prominent climatological feature across the high-latitude continental landmasses of the Northern Hemisphere during the cool season and are often associated with intense equatorward cold surges that can in turn have an adverse impact on the human population. These anticyclones are known to develop in response to a number of thermodynamical and dynamical factors. Early research has suggested that thermodynamic arguments (e.g., radiational cooling) could be employed to explain the development of these systems. Wexler (1937) described the effect of radiational cooling on surface pressure by demonstrating that when an air mass cools radiatively at low levels, isobaric surfaces are lowered aloft, and the compensating inflow of air at upper levels is associated with a rise in pressure at the surface. Curry (1987) demonstrated with an axisymmetric numerical model that surface pressure increases associated with anticyclogenesis are larger for an increased amount of cooling, as well as for cooling on large horizontal scales and at high latitudes. This model also showed that at a critical radius of less than 1000 km, approximately the Rossby radius of deformation, surface cooling contributes negligibly to pressure rises as inertia-gravity waves are readily generated to horizontally redistribute mass. Emanuel (2008) emphasized that complex thermodynamical processes related to polar anticyclogenesis, including radiational cooling, are poorly understood and necessitate further study.

Specific studies have addressed the relationship between autumn snow cover and the winter climate suggesting that the thermodynamic cooling effect of snow cover acts to influence large-scale circulation features including anticyclones. Ding and Krishnamurti (1987) analyzed the heat budget of the Siberian high and concluded that strong radiative cooling due in part to the snow-covered underlying surface was an important contributor to its rapid development. Foster

et al. (1983) examined autumn snow cover extent and its relationship with winter surface temperatures and found that autumn snow cover was more strongly correlated with the winter surface temperature over Eurasia than North America due to the relative size of the continental landmass. The snow-forced cold anomalies in autumn lead to the development of a persistent, strong anticyclone over Eurasia due to the large climatological extent of snow cover while the North American anticyclone is generally weaker and only becomes a more substantial feature when snow cover and subsequent cooling increases later in winter. Cohen and Entekhabi (1999) further demonstrate that anomalous autumn snow cover over Eurasia leads to positive surface pressure anomalies across Asia and North America in winter.

Although strong anticyclone formation is dependent on favorable thermodynamic conditions to some extent, dynamical factors have been shown to be critical to the development of these weather systems. For example, anticyclones are often observed to form during periods of atmospheric blocking. Many previous studies have revealed that upper-tropospheric blocking patterns, associated with episodes of high-latitude ridging, can promote the development of a strong surface anticyclone. These blocking patterns are established and enhanced through the poleward advection of anticyclonic vorticity within the warm sector of transient synoptic scale low-pressure systems. Namias (1945) focused on the relationship between cold-core polar anticyclogenesis and variations in the zonal index and observed that anticyclogenesis was more common during periods of low zonal index, associated with highly amplified trough-ridge patterns in the upper troposphere. Joung and Hitchman (1982) discussed the role of downstream development on East Asian cold surges by examining the growth and decay of upper-level height patterns across the Eurasian continent associated with Rossby wave trains. These anomalous height patterns originated over the North Atlantic Ocean as early as seven days prior to an

observed cold surge in East Asia. It was noted that the features were barotropic upstream of the surface anticyclone, however, transitioned to more of a baroclinic-type signature as they propagated downstream. Takaya and Nakamura (2005) expanded upon this research by identifying this particular wave train as a physical mechanism by which the Siberian high amplifies during the winter season. They indicated that the intraseasonal amplification of the Siberian high occurs in conjunction with a Rossby wave train that originates in the Atlantic basin, resulting in a blocking pattern across the Asian continent.

The formation of these upper-tropospheric blocking patterns has obvious dynamical implications for synoptic-scale subsidence coincident with the pressure rise associated with anticyclogenesis. In a study of strong anticyclogenesis over Alaska, Bodurtha (1952) observed that advection of cold air occurred from within the upstream ridge at 200 hPa. The convergence associated with this cold air advection was accompanied by subsidence in the lower and middle troposphere, contributing to the development of the anticyclone. Colucci and Davenport (1987) identified northwestern North America as a region where rapid anticyclogenesis is common. They also observed that strong anticyclogenesis in this region typically occurs in the cold air north of the primary 1000–500 hPa thickness gradient and is also associated with an upstream 500-hPa ridge amplification. Dallavalle and Bosart (1975) showed through two composite analyses that differential advection of anticyclonic vorticity, associated with horizontal velocity convergence in the upper troposphere, principally motivates subsidence resulting in anticyclonic tendencies consistent with the intensification of the composite surface anticyclones. Tan and Curry (1993) studied an intense anticyclone over North America that reached a central pressure of 1078 hPa occurring in late January and early February in 1989. They concluded in their analysis that vorticity advection and differential thermal advection were substantially more

important to the observed pressure rise with this particular anticyclone than were diabatic factors, including radiational cooling. They also showed that cold low-level air enhances anticyclogenesis by contributing positively to the differential thermal advection.

The goal of this study is to address some of the large-scale dynamical and thermodynamical differences associated with the formation of strong anticyclones over two climatologically favored regions, northwestern North America and central Asia, for strong anticyclone development during the Northern Hemisphere winter season. This paper aims to describe these features through a composite analysis of individual Alaskan and Siberian strong anticyclones. The paper is outlined as follows: Section 2 describes the methodology for selecting the individual anticyclone events for the composite analysis. Section 3 presents the results of the composite analyses of Alaskan and Siberian strong anticyclones. Section 4 discusses the relative importance of both dynamical and thermodynamical mechanisms in the development of Alaskan and Siberian anticyclones and the role of topography in their evolution. Section 5 concludes with a summary of the key differences observed between the Alaskan and Siberian composites.

2. Data and Methodology

Sea level pressure (SLP) is a common metric used to identify and track surface cyclones and anticyclones. The use of SLP in this manner carries with it a degree of uncertainty, especially over elevated terrain. Analysis schemes reduce a surface pressure to a sea level value under the assumption of a constant lapse rate between the surface and sea level and integrating the hydrostatic equation to mathematically solve for the SLP. This reduction to SLP can often lead to unrealistically large pressure gradients in areas where there is considerable variation in

elevation (Pauley 1998). The European Centre for Medium-Range Weather Forecasts (ECMWF) ERA-40 Reanalysis was selected for the composite analyses because of its global scope and it appears to have minimized the errors related to the reduction of surface pressure to SLP sufficiently for our purposes. Data were obtained from the ECMWF through the ERA-40 data server for the period 1 September 1957–31 August 2002.

The composite analyses of individual strong anticyclone events were created for the winter season, defined here to be the period November–March, for the years 1978/79 through 2001/02. The integration of a larger volume of satellite-derived data into the ERA-40 dataset since 1979 was the primary reason for the selection of this period. Uppala et al. (2005) provides a more complete discussion on the marked improvement in the quality of the ERA-40 following the introduction of this satellite data. An annual frequency map of SLP values of 1050 hPa or greater was created by counting the number of times a 1050 hPa SLP value was observed at each Northern Hemisphere grid point at 0000 and 1200 UTC for the full 45-year period of the ERA-40. The 1050 hPa SLP frequency maxima were identified and these points were used to determine the geographical domain for the composites. The individual anticyclone events comprising the composites were identified by searching a 15° X 15° grid at 2.5° intervals centered on the location of the 1050 hPa SLP frequency maxima over northwestern North America (62.5°N, 135°W) and central Asia (50°N, 95°E). A threshold of 1050 hPa was selected as the minimum SLP threshold for the Alaskan composite and 1060 hPa was selected for the Siberian composite, both of which represent a SLP value that is approximately 2.5 standard deviations greater than the climatological value for each region. These thresholds were designated to ensure that a sufficient number of events were selected for analysis, yet still were representative of a strong anticyclone for each region. The composites were centered (t = 0) at

the time of the maximum SLP. Anomaly fields were calculated as a departure from the November–March mean value.

The primary diagnostic equation used to quantitatively evaluate the dynamical forcing for vertical motion in the composite analyses is the **Q**-vector form of the quasi-geostrophic omega equation. **Q** and the divergence of **Q** are defined similarly to Bluestein (1992):

$$\vec{\mathbf{Q}} = -\frac{R}{\sigma p}\left(\begin{array}{c}\frac{\partial \vec{\mathbf{V}}_g}{\partial x}\bullet\vec{\nabla}_p T \\ \frac{\partial \vec{\mathbf{V}}_g}{\partial y}\bullet\vec{\nabla}_p T\end{array}\right) \qquad (1)$$

$$\left(\vec{\nabla}_p{}^2 + \frac{f_0{}^2}{\sigma}\frac{\partial^2}{\partial p^2}\right)\omega \approx -2\vec{\nabla}_p \bullet \vec{\mathbf{Q}} \qquad (2)$$

where R is the dry gas constant, σ is a static stability coefficient, $\mathbf{V}_g$ is the geostrophic wind, ∇_p is the horizontal gradient operator along a constant pressure surface, T is temperature, and f_0 is a constant reference value of the Coriolis parameter. The divergence of **Q** is directly proportional to the forcing for vertical motion at a given pressure level with convergence (divergence) of **Q** associated with ascent (descent). As applied in the composite analysis performed in this study, **Q**-vectors were calculated every 100 hPa for a 500–700 hPa layer and then averaged to evaluate the spatial distribution and relative strength of the forcing for subsidence in the troposphere.

Surface energy flux data were also examined to show thermodynamic changes at the surface leading up to the maximum SLP in each composite anticyclone. The surface energy balance equation that was used is as follows:

$$L_{net} = SSR + STR + SLHF + SSHF$$

where L_{net} is the net surface energy flux, SSR is the net solar radiation at the surface, STR is the net thermal radiation at the surface, and SLHF and SSHF are the turbulent fluxes of latent and sensible heat, respectively.

3. Results

a. Annual Frequency of SLP 1050 hPa or greater

The mean November–March SLP for the period 1957–2002 is shown in Figure 1a. The dominant features include a distinct SLP maximum over central Asia and strong cyclonic signatures in both the North Atlantic and North Pacific Oceans. The mean SLP over northwestern North America is significantly lower compared with central Asia. Figure 1b shows the annual frequency of SLP values 1050 hPa or greater for the period 1 September 1957–31 August 2002. The frequency of 1050 hPa SLP values is greatest over the continental landmasses poleward of 40°N and over the snow- and ice-covered surfaces of the Arctic Ocean. The maximum annual frequency in the Northern Hemisphere is located along the northwestern border of Mongolia, west-southwest of Lake Baikal, observing a 1050 hPa SLP approximately 19 times per year. It is also apparent that strong anticyclone occurrence is substantially influenced by topography as evidenced by relative 1050 hPa frequency maxima to the east of major terrain features, especially the Rocky Mountains in western Canada. The Tibetan Plateau also greatly influences the location of strong anticyclones over central Asia by limiting their equatorward extent as indicated by the sharp decline in the 1050 hPa frequency near 40–45°N in central Asia.

b. Alaskan Composite

The geopotential height sequence at 300 hPa for the 21-member (see Table 1) Alaskan composite is shown in Figure 2. At $t = -2$ days relative to the time of the maximum SLP, a low amplitude ridge-trough pattern exists over the eastern Pacific and western North America with positive and negative height anomalies encompassing the ridge and downstream trough, respectively (Fig. 2a). The ridge at 300 hPa becomes highly amplified with a slight negative tilt by $t = 0$, extending poleward over the Arctic Ocean (Fig. 2b). The corresponding height anomalies at this time are greater than 400 m in the ridge over western Alaska. The downstream trough deepens between $t = -2$ days and $t = 0$ with negative 300-hPa height anomalies less than −200 m spreading westward to near the Pacific coast. The development of the 300-hPa ridge over Alaska is associated with a strong, zonally-oriented 60 m s^{-1} jet located off the east coast of Asia extending over the western North Pacific (Fig. 3). A 30 m s^{-1} jet curves southeastward over western Canada, becoming positioned west to east over the contiguous United States. Cold-air advection just to the east of the major ridge axis is contributing to a maximum in the horizontal velocity convergence in the poleward entrance region greater than 1.8 X 10^{-5} s^{-1}, just to the east of the major ridge axis. This convergence maximum is positioned over the center of the surface anticyclone at $t = 0$.

A surface low pressure is located just west of the Aleutian Islands at $t = -2$ days with a weak pressure ridge over Alaska and northwestern Canada (Fig. 4a). The anticyclone becomes a closed feature in the SLP field by $t = -1$ day (Fig. 4b). The upstream surface low has strengthened and a large pressure gradient develops between the surface low and the incipient anticyclone, oriented approximately normal to the 1000–500 hPa thickness gradient. This implies that strong warm-air advection is occurring in the lower troposphere west of Alaska, contributing to the ridge amplification described earlier. The surface low remains positioned

west of the Aleutians by $t = 0$ indicating that the warm-air advection persisted through the period of anticyclogenesis (Fig. 4c). The 1000–500 hPa thickness anomalies indicate that a cold low-level air mass begins to advect southward at $t = -2$ days with the lowest 1000–500 hPa thicknesses located over northern Canada. As the anticyclone strengthens, the associated flow to its southeast is directed southwestward against the elevated terrain of the Rockies, continuing to advect colder air from northern Canada. The low-level cold air is positioned farther south by $t = 0$ as evidenced by 1000–500 hPa thickness anomalies of less than −18 dam over eastern British Columbia and western Alberta.

c. Siberian Composite

The geopotential height pattern at 300 hPa for the 17-member (see Table 2) Siberian composite is distinct from the Alaskan composite in both amplitude and orientation. A positively-tilted ridge at 300 hPa, extending from southwest to northeast over central Asia at $t = -2$ days, is associated with positive height anomalies of greater than 200 m (Fig. 5a). The positive height anomalies in the ridge increase slightly by $t = 0$, however, are still roughly half of the magnitude of the positive height anomalies associated with the ridge at the analogous time in Alaskan composite (Fig. 5b). The ridge-trough pattern deamplifies slightly between $t = -2$ days and $t = 0$ as the trough begins to lift northeastward. A broad 50 ms^{-1} jet at 300 hPa is located off the Asian coast just south of the Korean peninsula and Japan at $t = 0$ (Fig. 6). Cold-air advection appears to be considerably weaker than in the Alaskan composite as the flow weakens near the trough axis and becomes oriented normal to the thermal gradient farther downstream. The associated horizontal velocity convergence in the poleward entrance region of the jet is also

approximately half of the value in the Alaskan composite, maximizing at just over 9.0 X 10^{-6} s^{-1}, and is similarly positioned near the center of the surface anticyclone at $t = 0$.

A surface anticyclone is located over a large region encompassing most of central Asia at $t = -2$ days in the Siberian composite (Fig. 7b). A surface low pressure is located upstream over the Arctic Ocean in conjunction with the incipient surface anticyclone. Although it is persistent as in the Alaskan composite, the 1000–500 hPa thickness anomalies at $t = 0$ suggest that the warm air advection is generally weaker, as the anomalies are more limited in both extent and magnitude. The difference in the strength of the low-level warm advection between the two composites may relate to the observed changes in the amplitude of the ridge upstream of the developing anticyclone between $t = -2$ days and $t = 0$. Low-level cold air is advected in close proximity to the center of the Siberian anticyclone. The 1000–500 hPa thickness anomalies indicate that the anomalous cold air is also present earlier (compare Figs. 4a and 7a) and the anomalies are generally larger overall despite being similar to those found in the Alaskan composite at $t = 0$. The surface flow associated with the Siberian anticyclone differs from the Alaskan anticyclone in that the flow is directed along the elevated terrain in northeastern China and extending west adjacent to the Tibetan plateau. The 1000–500 hPa thickness contours along the elevated terrain suggests that cold advection at low levels is weaker to the south and east of the Siberian anticyclone.

d. Tropospheric forcing for large-scale subsidence

Q-vectors analyses for a 500–700 hPa layer were calculated for the Alaskan and Siberian composites to assess the mid-level quasi-geostrophic forcing for subsidence associated with anticyclogenesis. The comparison of **Q**-vectors and **Q**-vector divergence in the Alaskan

composite at $t = -1$ day and $t = 0$ appears in Fig. 8. The **Q**-vectors indicate the presence of a strong vertical circulation associated with the jet entrance regions as they cross the thermal gradient from cold to warm air. This pattern is consistent with horizontal velocity convergence resulting from anticyclonic vorticity advection and cold-air advection centered over the incipient surface anticyclone. At $t = -1$ day, the magnitude of the maximum **Q**-vector divergence is similar for both composites (approximately 3.0 X 10^{-12} Pa m^{-2} s^{-1}), with the maximum divergence of **Q** located slightly farther west relative to the position of the surface anticyclone in the Siberian composite (compare Figs. 8a and 9a). The differences between the Alaskan and Siberian composites become more evident by $t = 0$. The Alaskan composite exemplifies strong dynamical forcing in the 500–700 hPa layer with strong **Q**-vector divergence, maximizing at near 6.0 X 10^{-12} Pa m^{-2} s^{-1}, in a region just southeast of the anticyclone center at the time of maximum SLP (Fig. 8b). In contrast, the forcing for subsidence associated with the Siberian composite has weakened at $t = 0$ (Fig. 9b). Additional **Q**-vector analyses in the 700–850 hPa layer (not shown) at $t = 0$ further demonstrate that forcing for subsidence is stronger at levels below 700 hPa in the Alaskan composite. The **Q**-vectors remain directed from cold to warm air at low levels indicating a tightening of the thermal gradient and strong ageostrophic flow associated with the vertical circulation in the jet entrance region. The **Q**-vector divergence, however, is comparatively weak and disorganized in the 700–850 hPa layer in the Siberian composite.

Vertical cross-sections were constructed at $t = -1$ day for each composite to relate the calculated **Q**-vector forcing to its impact on vertical motion in the troposphere. The analyzed ERA-40 vertical velocities associated with the Alaskan composite are generally greater with maximum values reaching 2.8 X 10^{-3} hPa s^{-1} in the mid-troposphere at approximately 500 hPa

(Fig. 10a). At $t = -1$ day, the vertical velocities observed with the Siberian composite are noticeably weaker by almost a factor of two with maximum values only reaching 1.6 X 10^{-3} hPa s^{-1} (Fig. 10b). The vertical velocity fields allow us to see the depth of strong descent found in the Alaskan composite indicative of the strong dynamical forcing in the mid and upper troposphere. The unfavorable folded over orientation of the pressure ridge in Siberia as well as its distance from the upper level jet dynamics are apparent in the vertical velocity over this region as it is roughly half the magnitude as found in the Alaskan composite. As shown in the **Q**-vector diagnostics, dynamical forcing strengthens in the Alaskan composite by $t = 0$, however, becomes weaker and more disorganized in the Siberian composite. The associated vertical velocity patterns support the conclusion that subsidence due to dynamical processes in the mid and upper troposphere is of greater importance to the development of the Alaskan anticyclone.

e. Surface Energy Fluxes

The Alaskan and Siberian anticyclones experienced SLP increases between $t = -4$ days and $t = 0$ that were remarkably similar despite the clear difference in the amplitude of the upstream ridges at 300 hPa. The role of near-surface cooling in the SLP rise associated with each anticyclone was examined by calculating the center-differenced 24-h change in the potential temperature at 925 hPa and this was compared to the net surface energy flux. The 24-h potential temperature change at 925 hPa in the Alaskan composite is significantly larger at $t = 0$, reaching −6 K southeast of the anticyclone center, consistent with the advance of cold air as observed in the 1000–500 hPa thickness field (Figs. 11a, b). The decrease in the potential temperature at 925 hPa is also consistent with the **Q**-vector pattern associated with a strengthening of the thermal gradient. The net surface energy flux was largely negative for both times in the Alaskan

composite, indicative of cooling, from $t = -2$ days to $t = 0$ (Figs. 11c, d). Analysis of individual terms in the surface energy balance equation (not shown) show that the net flux is dominated by a negative sensible heat flux, presumably due to advection of cold air from northern Canada.

A 24-h potential temperature change at 925 hPa of −4K in the Siberian composite occurs very near the center of the anticyclone at $t = -2$ days (Fig. 12a). At $t = 0$, the potential temperature has lowered southeast of the anticyclone center, but to a certain extent this decrease is confined north and west of the elevated terrain in northeast China (Fig. 12b). The net surface energy flux at both times is also negative except north of the surface anticyclone in north central Asia (Fig. 12c, d). The dominant term in the surface energy balance equation for the Siberian composite is a strongly negative net thermal radiation flux term, consistent with the expectation of strong radiative cooling in the region.

4. Discussion

Radiative and dynamical processes play distinctive roles in strong anticyclone formation. Radiative forcing acts on long time scales resulting in a slow, but steady increase in SLP as an air mass cools over a period of several days or weeks. In general, dynamical forcings associated with transient synoptic scale weather systems are apt to be more robust and can be accompanied by large increases in SLP on short time scales, typically ranging from a day to several days. A strong anticyclone as defined by the SLP thresholds set forth in this paper are found likely to result from a combination of these processes.

From a broad climatological perspective, the strong Alaskan anticyclone occurs less frequently than the strong Siberian anticyclone. The annual frequency of a SLP 1050 hPa or greater over the northwestern North America is approximately an order of magnitude less than

the annual frequency observed over central Asia (see Fig. 1) with values of 1-2 per year over the former with nearly 20 per year observed over the latter. Takaya and Nakamura (2005) have indicated that the Siberian high is a semipermanent feature with a central SLP exceeding 1030 hPa during the winter season. Unsurprisingly, in the November–March mean (Fig. 1a), a closed SLP feature resembling the Siberian anticyclone is apparent over central Asia, however, over northwestern North America an analogous closed feature does not exist. The frequency with which strong Alaskan and Siberian anticyclones form is likely a result of the relative efficiency in establishing and maintaining a cold air mass for a given period of time over the respective regions. As indicated by Foster et al. (1983), snow cover and subsequent cooling occurs much earlier and persists longer over central Asia than over North America, and this is presumably an important distinction that can partially explain the difference in the observed frequency of strong anticyclones over these regions. The proximity of the Alaskan domain to the Pacific and Arctic Ocean basins would also appear to contribute negatively to the maintenance of a cold air mass, as advection of marine air masses over northwestern North America will tend to limit the length of any period of radiative cooling. For this reason, we speculate that the formation of a strong Alaskan anticyclone is more likely to require a specific anticyclogenesis sequence dominated by upstream ridge amplification.

The dynamical basis for an anticyclogenesis sequence associated with the development of a large amplitude ridge-trough pattern is well understood. The advection of warm air into a ridge, typically with a surface low pressure located to the west of the ridge, leads to a positive height tendency within the ridge above the maximum in warm air advection. This positive height tendency is accompanied by a negative vorticity tendency and cold anomaly in the upper ridge. Another important component to the development of a strong anticyclone is an antecedent

cold air mass over the region of anticyclone formation. A positive height tendency follows cold air advection or radiative cooling near the surface as the low-level air mass cools. This height tendency results in a negative vorticity tendency within the thermal trough that develops over the region of cooling. The cooling also results in the initial SLP rise. The amplification of the ridge-trough pattern associated with anticyclogenesis increases the vorticity gradient between the ridge and trough implying a subsequent increase in the differential anticyclonic vorticity advection over the surface anticyclone. The end result of this process is strong anticyclogenesis located approximately at the inflection point between the ridge and trough associated with substantial tropospheric subsidence.

The upstream ridge amplification associated with the development of the strong Alaskan anticyclone is rather significant. The position of the ridge axis shifts slightly eastward between $t = -1$ day and $t = 0$. The ridge and the downstream trough amplify between $t = -1$ day and $t = 0$ accompanied by a decrease in the half wavelength between the ridge and trough over Alaska and northwest Canada. This decrease in the half wavelength supports the assertion that dynamical forcing is especially important to the Alaskan anticyclone. The result of strong differential anticyclonic vorticity advection is an implied increase in convergence associated with subsidence below. **Q**-vector divergence is strongly maximized at the inflection point near the anticyclone center, and subsequently, the subsidence associated with the Alaskan anticyclone is much stronger throughout the depth of the troposphere especially below 500 hPa as compared with the Siberian anticyclone (Fig. 10b). The ridge is observed to be more transient in the Siberian composite. This behavior is similar to that described by Takaya and Nakamura (2005) who show that a blocking ridge associated with the quasi-stationary Atlantic wave train stimulates a SLP rise in the Siberian high. The downstream development of the ridge-trough pattern associated

with the Siberian anticyclone leads to a shorter period of dynamical forcing resulting in subsidence. This relatively short period of forcing is exemplified in the **Q**-vector analyses. The maximum **Q**-vector divergence occurs at $t = -1$ day and tends to relax thereafter which is indicative of the transient nature of the blocking pattern over the Eurasian continent also described by Joung and Hitchman (1982) as the ridges and troughs grow and decay while propagating downstream.

The net surface energy flux was observed to be largely similar between the Alaskan and Siberian composites at $t = 0$ which was somewhat of an unexpected result because the observed anticyclogenesis rate in both composites was comparable despite differences with regard to the impact of the upstream ridge. At $t = 0$, the negative fluxes and associated cooling have progressed along the eastern slopes of the Rockies in the Alaskan composite and toward the coast near China in the Siberian composite, respectively. A subtle difference is that there is an area of cooling located just to the south and west of the center of the anticyclone in the Siberian composite, which could account for a portion of the observed pressure rise at the anticyclone center. Although not explicitly addressed in this paper, it is reasonable to assume that cooling leading up to development of the Siberian anticyclone is also greater (prior to $t = -4$ days) given that there is a significant cold anomaly evident in the 1000–500 hPa thickness anomaly field at $t = -4$ days (Fig. 7a) in the Siberian composite that does not exist in the Alaskan composite.

The interaction of low-level cold air with the regional topography also plays a critical role in the development of both the Alaskan and Siberian anticyclones. The Alaskan anticyclone develops northeast of the Alaska Range and Canadian Rockies with the negative 1000–500 hPa thickness anomalies to the southeast along the eastern slopes of the Rockies. With the elevated terrain primarily confined to the south and west of the Alaskan anticyclone, cold air associated

with the system is relatively unobstructed and can move equatorward along the eastern edges of the Rockies. The progression of the Siberian anticyclone appears to be a bit slower than the Alaskan anticyclone perhaps indicating that the topography may play a greater role in modulating the movement of Siberian anticyclones. The topography surrounding each of the composite anticyclones is complex and contributes greatly to their evolution, but may also factor into the relative frequency with which a strong anticyclone is observed over each region. The terrain affects the movement of the cold air and the pressure field associated with it. The difference in the orientation of the topography over each region suggests that the dynamical component to the development of the Alaskan anticyclone may be of necessarily greater importance than for the Siberian anticyclone because the cold air associated with the Siberian anticyclone is obstructed in its equatorward movement until it reaches the eastern portion of the Tibetan plateau. The cold air associated with the Alaskan anticyclone, however, can move equatorward more quickly without a physical boundary to limit its movement.

5. Conclusions

Composite analyses of strong anticyclones over Alaska and Siberia were performed. The development of the strong Alaskan anticyclone is associated with a highly amplified ridge-trough pattern at 300 hPa. Anticyclonic vorticity advection and cold-air advection over the incipient surface anticyclone accompanies strong subsidence over the depth of the troposphere. The strong Siberian anticyclone develops under a less dynamically favorable ridge-trough pattern with 300 hPa height anomalies roughly half of the value of those found in association with the Alaskan anticyclone. The vertical velocities associated with the formation of the Siberian anticyclone were less substantial than those found with the Alaskan anticyclone. In addition to

the dynamical characteristics, the interaction of cold air with complex topography contributes greatly to the observed behavior of each composite anticyclone. The Alaskan anticyclone forms primarily east of the Rockies and cold air associated with it tends to move equatorward, as its movement is not restricted by a physical boundary. The cold air is accompanied by a higher SLP and, consequently, as the cold air mass shifts equatorward, the anticyclone extends to the south and east. The Siberian anticyclone develops surrounded by regions of high terrain north of the Tibetan plateau, which does not facilitate the equatorward movement of cold air as easily as observed with the Alaskan anticyclone.

Acknowledgements

This research was conducted at the University at Albany as part of the first author's M.S. Thesis under support from NSF Grant ATM-0434189. We would like to thank Lance Bosart, Daniel Keyser, and an anonymous reviewer for their helpful comments and suggestions. Cohen is supported by NSF Grants ARC-0909457 and ARC-0909459.

REFERENCES

Bluestein, H. B., 1992: *Principles of Kinematics and Dynamics*. Vol. I. *Synoptic-Dynamic Meteorology in Midlatitudes*. Oxford University Press, 431 pp.

Bodurtha, F. T., 1952: An investigation of anticyclogenesis in Alaska. *J. Atmos. Sci.*, **9**, 118–125.

Cohen, J., and D. D. Entekhabi, 1999: Eurasian snow cover variability and Northern Hemisphere climate predictability. *Geophys. Res. Lett.*, **26**, 345–348.

Colucci, S. J., and J. C. Davenport, 1987: Rapid surface anticyclogenesis: Synoptic climatology and attendant large-scale circulation changes. *Mon. Wea. Rev.*, **115**, 822-836.

Curry, J., 1987: The contribution of radiative cooling to the formation of cold-core anticyclones. *J. Atmos. Sci.*, **44**, 2575–2592.

Dallavalle, J. P., and L. F. Bosart, 1975: A synoptic investigation of anticyclogenesis accompanying North American polar air outbreaks. *Mon. Wea. Rev.*, **103**, 941–957.

Ding, Y., and T. N. Krishnamurti, 1987: Heat budget of the Siberian high and the winter monsoon. *Mon. Wea. Rev.*, **115**, 2428–2449.

Emanuel, K., 2008: Back to Norway: An essay. *Synoptic–Dynamic Meteorology and Weather Analysis and Forecasting: A Tribute to Fred Sanders, Meteor. Monogr.,* No. 55, Amer. Meteor. Soc., 440 pp.

Foster, J., M. Owe, and A. Rango, 1983: Snow cover and temperature relationships in North America and Eurasia. *J. Climate Appl. Meteor.*, **22**, 460–469.

Joung, C. H., and M. H. Hitchman, 1982: On the role of successive downstream development in East Asian polar air outbreaks. *Mon. Wea. Rev.*, **120**, 1224–1237.

Namias, J., 1945: Investigation of polar anticyclogenesis and associated variation of the zonal index. U.S. Weather Bureau Research Paper No. 24, 22 pp.

Pauley, P. M., 1998: An example of uncertainty in sea level pressure reduction. *Wea. Forecasting*, **13**, 833-850.

Takaya, K., and H. Nakamura, 2005: Mechanisms of intraseasonal amplification of the cold Siberian high. *J. Atmos. Sci.*, **62**, 4423–4440.

Tan, Y. C., and J. A. Curry, 1993: A diagnostic study of the evolution of an intense North American anticyclone during winter 1989. *Mon. Wea. Rev.*, **121**, 961–975.

Uppala, S. M., and Coauthors, 2005: The ERA-40 Re-Analysis. *Quart. J. Roy. Meteor. Soc.,* **131**, 2961–3012.

Wexler, H., 1937: Formation of polar anticyclones. *Mon. Wea. Rev.*, **65**, 229-236.

LIST OF FIGURES

FIG. 8. 500–700 hPa column-averaged **Q**-vectors and **Q**-vector divergence (positive values shaded every 1.0 X 10^{-12} Pa m^{-2} s^{-1}), 500–700 hPa layer mean heights (solid contours, dam), and temperature (dashed, K) at (a) $t = -1$ day and (b) $t = 0$ for the Alaskan composite. A bold 'H' denotes the location of the surface anticyclone center.

FIG. 9. As in FIG. 8, except for the Siberian composite.

FIG. 10. Vertical cross-sections of ω (thicker contours, X 10^{-3} hPa s^{-1}) and winds (m s^{-1}) at $t = -1$ day for the Alaskan composite (top) and Siberian composite (bottom).

FIG. 11. SLP (solid contours, hPa) and 24-h difference of 925-hPa θ (shaded) centered at (a) $t = -2$ days and (b) $t = 0$ for the Alaskan composite. Net surface energy flux (W m^{-2}) at (c) $t = -2$ days and (d) $t = 0$.

FIG. 12. As in FIG. 11, except for the Siberian composite.

TABLE 1. The dates and maximum ERA-40 SLP for individual anticyclone events included in the Alaskan composite.

Time (UTC) / Date	ERA-40 SLP (hPa)
0000 / 18 November 1978	1052.63
1200 / 03 January 1979	1053.34
1200 / 08 January 1980	1050.60
0000 / 26 January 1980	1057.92
1200 / 18 December 1980	1062.00
1200 / 24 February 1982	1056.17
0000 / 22 December 1983	1059.04
1200 / 09 November 1985	1054.38
1200 / 21 November 1985	1054.02
0000 / 03 January 1989	1070.64
1200 / 18 December 1990	1053.19
0000 / 03 January 1991	1053.28
1200 / 25 January 1991	1050.43
0000 / 28 December 1992	1055.62
1200 / 21 February 1994	1054.13
0000 / 12 February 1995	1053.76
1200 / 07 December 1995	1050.12
0000 / 03 March 1996	1053.96
0000 / 12 March 1997	1054.20
1200 / 18 December 1998	1067.45
0000 / 05 March 2002	1055.69

TABLE 2. The dates and maximum ERA-40 SLP for individual anticyclone events included in the Siberian composite.

Time (UTC) / Date	ERA-40 SLP (hPa)
0000 / 13 January 1979	1062.24
1200 / 16 November 1979	1062.85
1200 / 03 February 1980	1061.44
0000 / 25 January 1981	1060.64
0000 / 17 December 1981	1061.95
0000 / 22 December 1984	1062.63
1200 / 26 November 1987	1074.36
1200 / 13 February 1988	1063.69
0000 / 03 March 1989	1065.47
0000 / 22 January 1990	1061.63
0000 / 29 November 1990	1063.63
0000 / 18 January 1991	1064.24
1200 / 15 December 1993	1062.57
0000 / 19 February 1996	1064.57
1200 / 04 December 1996	1062.36
1200 / 23 January 2000	1060.76
0000 / 19 December 2001	1060.49

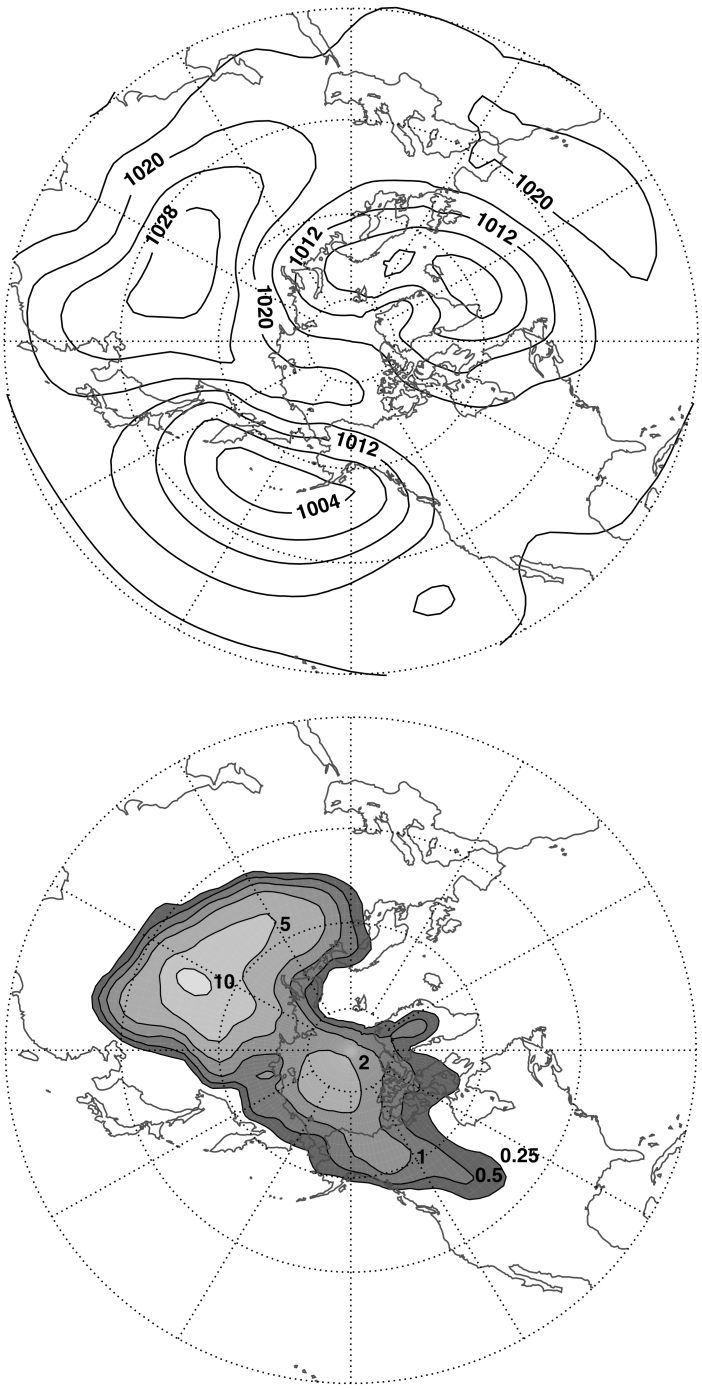

FIG. 1. Mean November–March SLP for the period 1957–2002 (top) and annual frequency of observed SLP values greater than or equal to 1050 hPa (bottom).

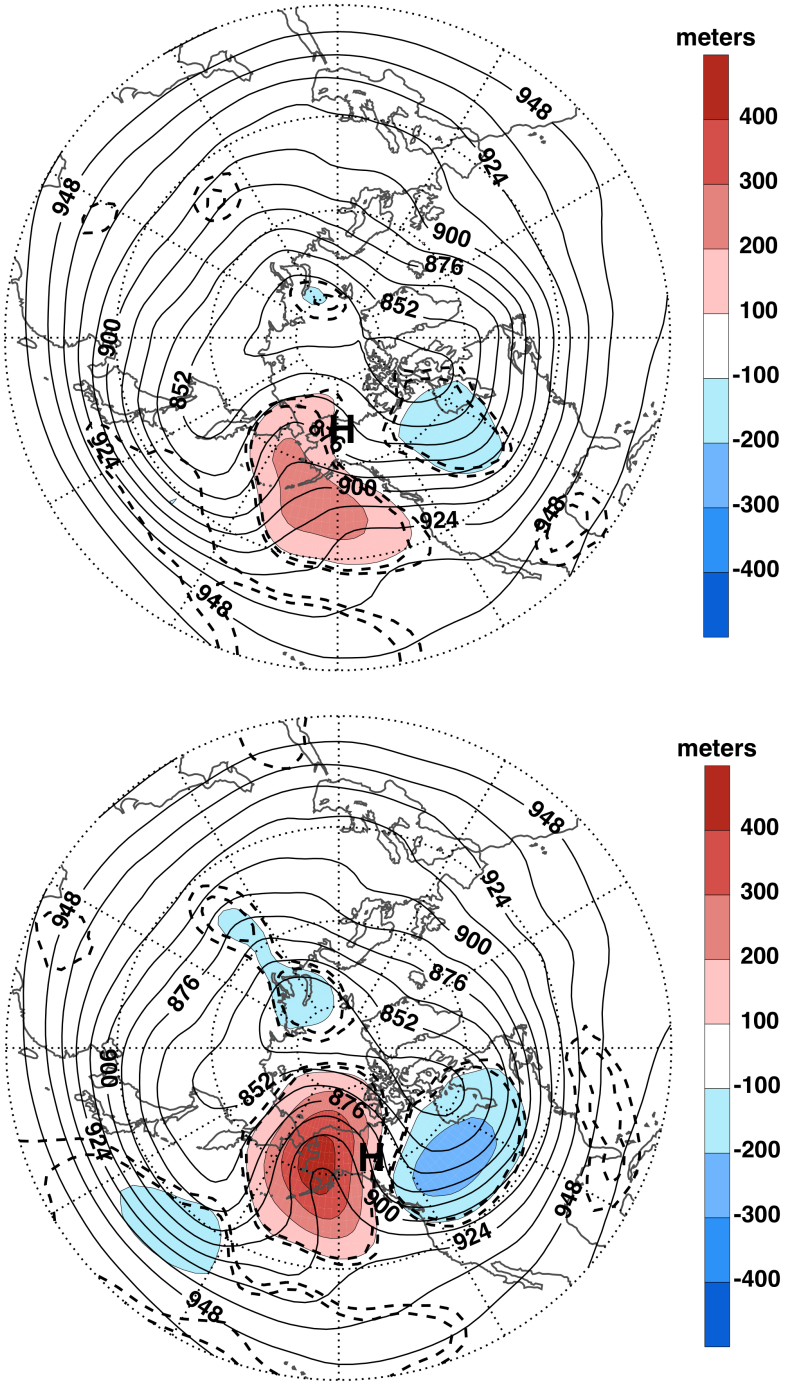

FIG. 2. 300 hPa geopotential heights (solid contours, dam) and height anomalies at $t = -2$ days (top) and at $t = 0$ (bottom) for the Alaskan composite. The anomalies that are statistically significant at the 95% and 99% levels are dashed. A bold 'H' denotes the location of the surface anticyclone center.

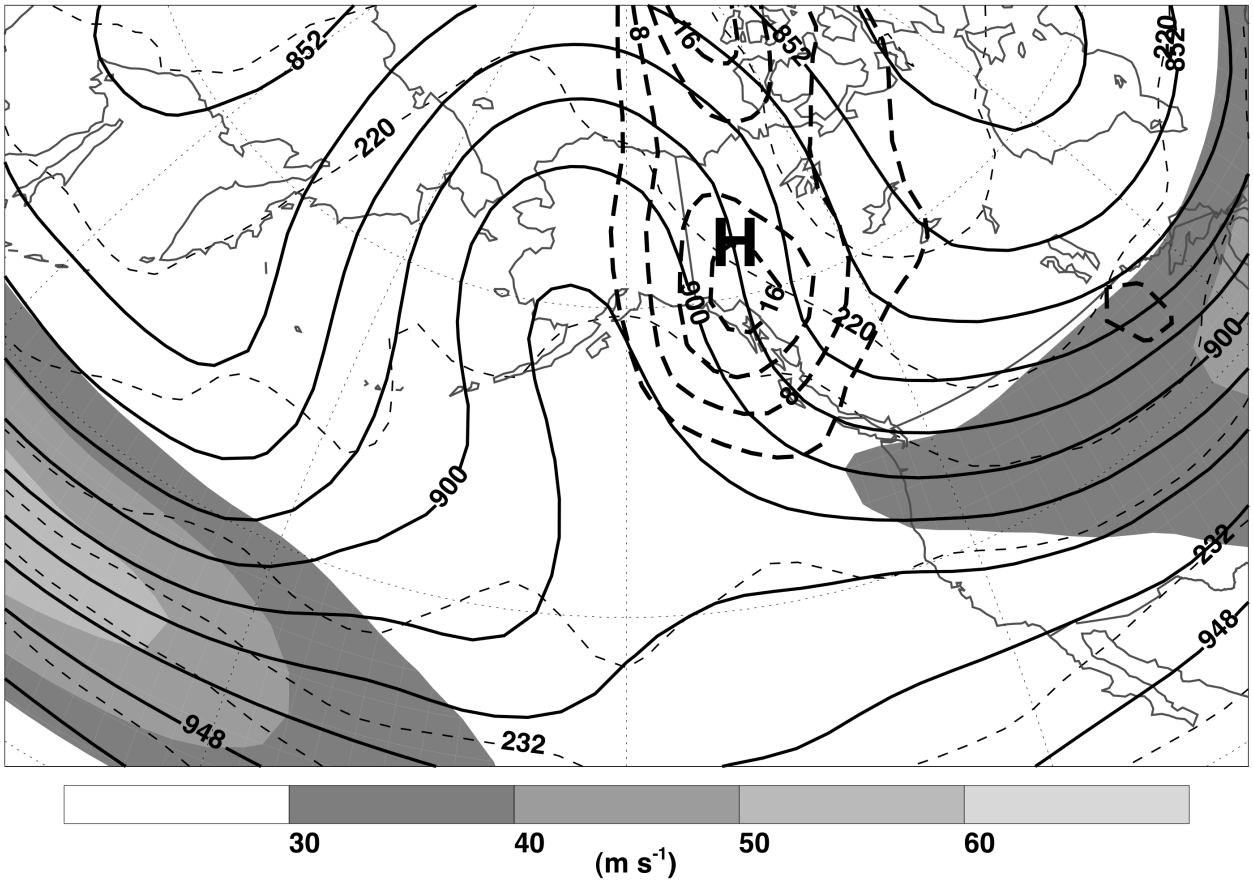

FIG. 3. 300 hPa geopotential heights (solid contours, dam), temperature (short dashes, K), wind speed (shaded, m s^{-1}), horizontal velocity convergence (long dashes, X 10^{-6} s^{-1}) at $t = 0$ for the Alaskan composite. A bold 'H' denotes the location of the surface anticyclone center.

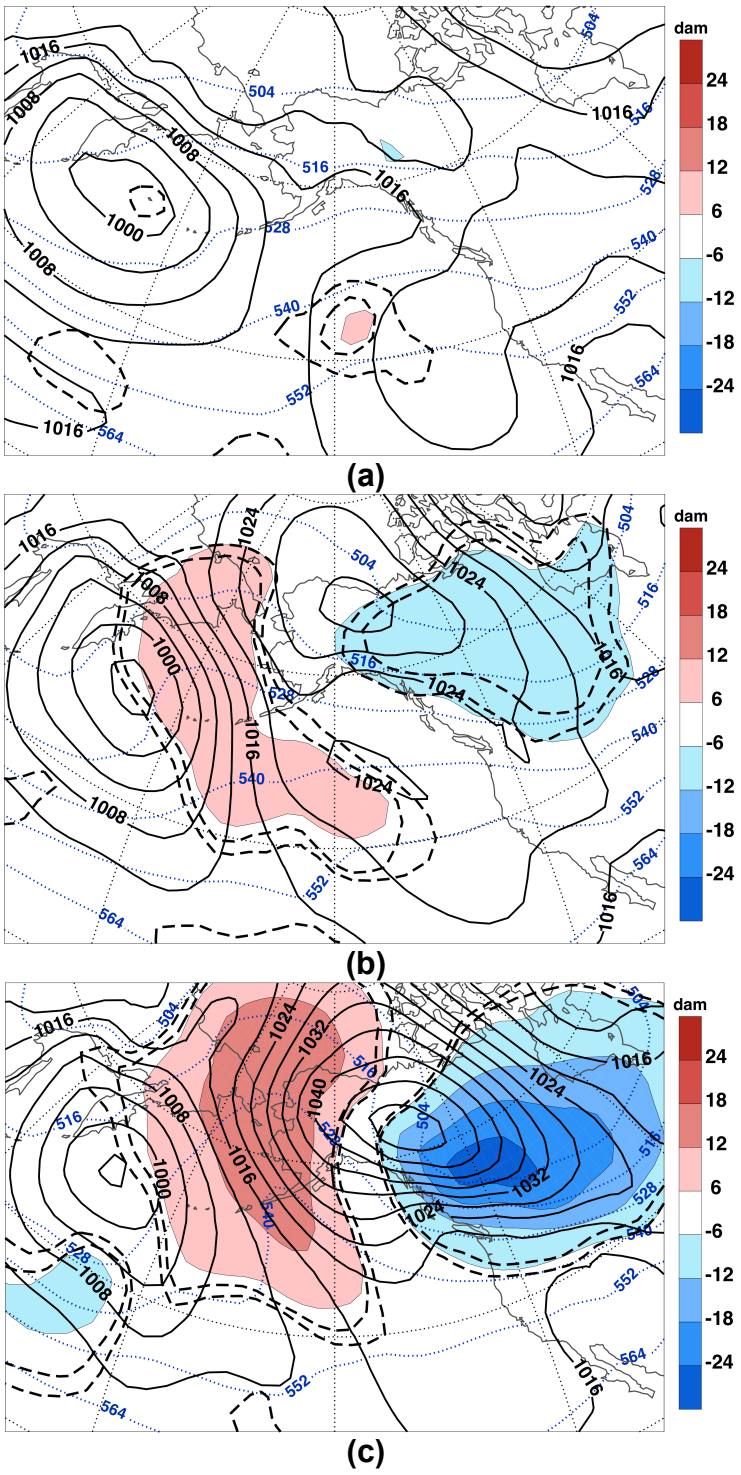

FIG. 4. (a) SLP (solid contours, hPa), 1000–500 hPa thickness (dotted, dam) and 1000–500 hPa thickness anomalies (shaded, dam) at (a) $t = -4$ days, (b) $t = -2$ days, and at (c) $t = 0$ for the Alaskan composite. The anomalies that are statistically significant at the 95% and 99% levels are dashed.

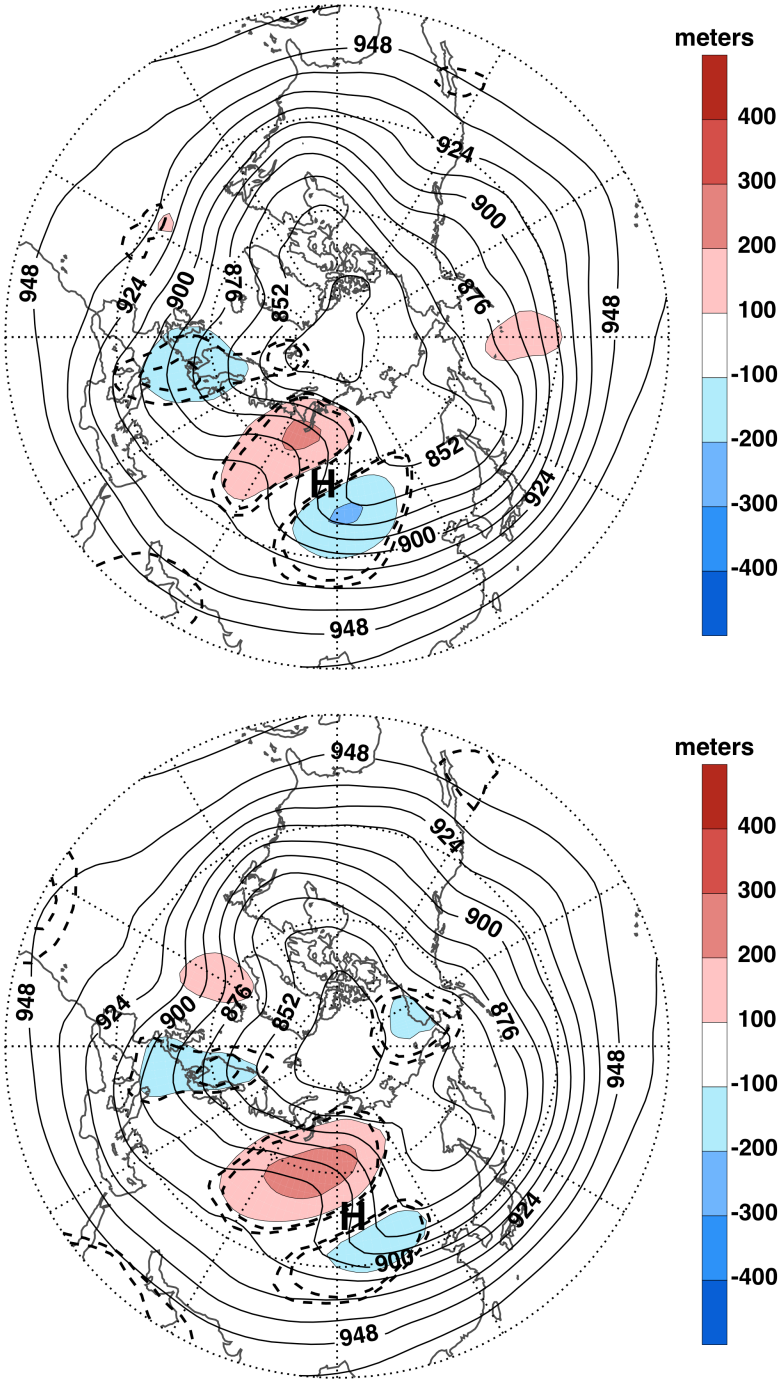

FIG. 5. As in FIG. 2, except for the Siberian composite.

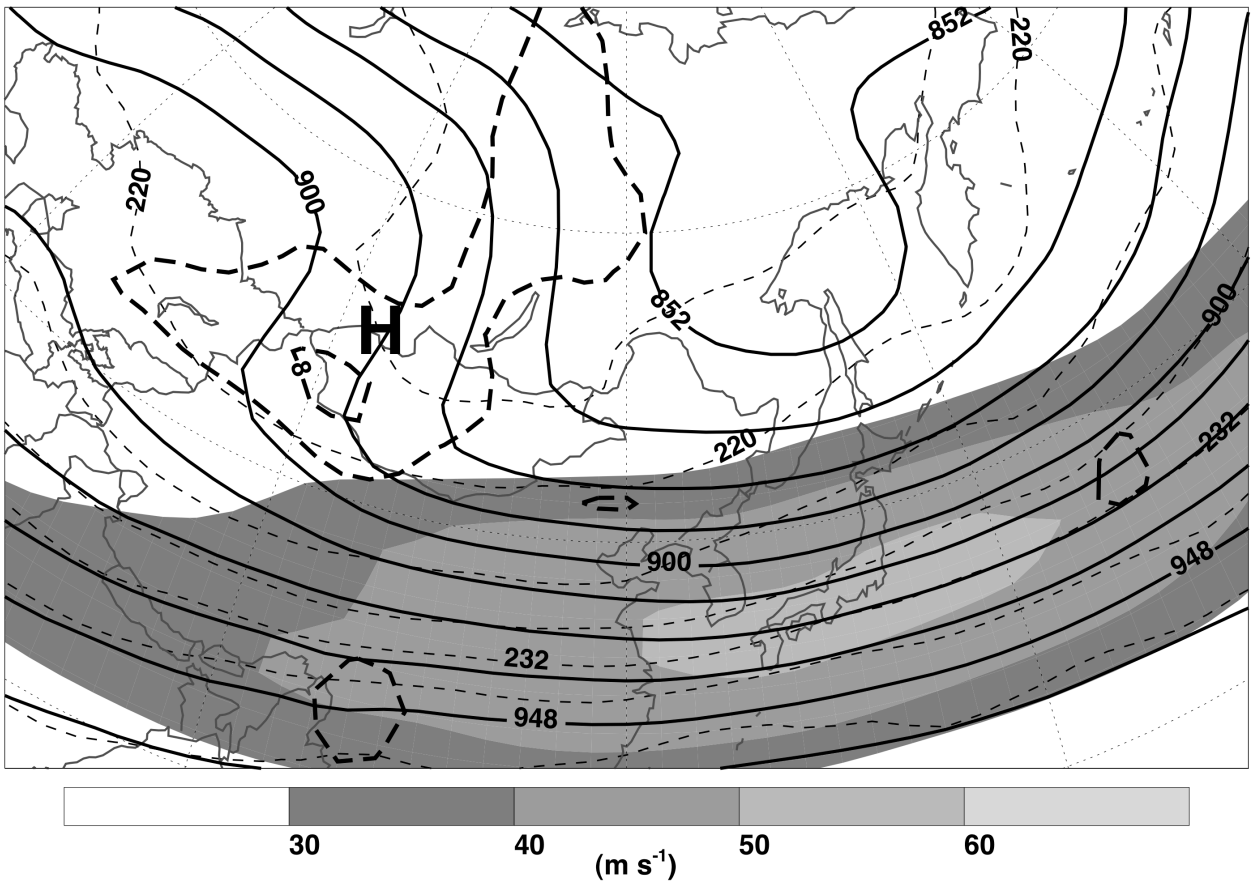

FIG. 6. As in FIG. 3, except for the Siberian composite.

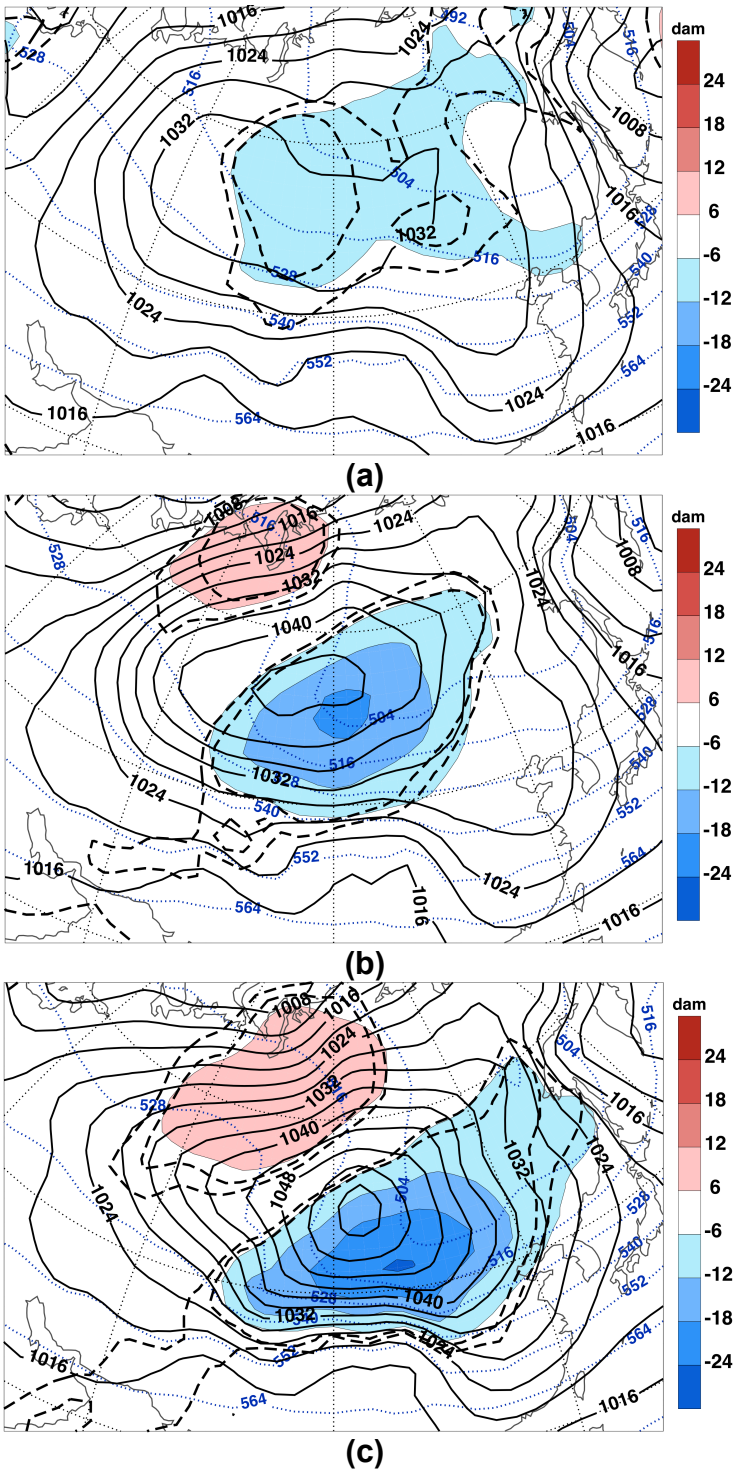

FIG. 7. As in FIG. 4, except for the Siberian composite.

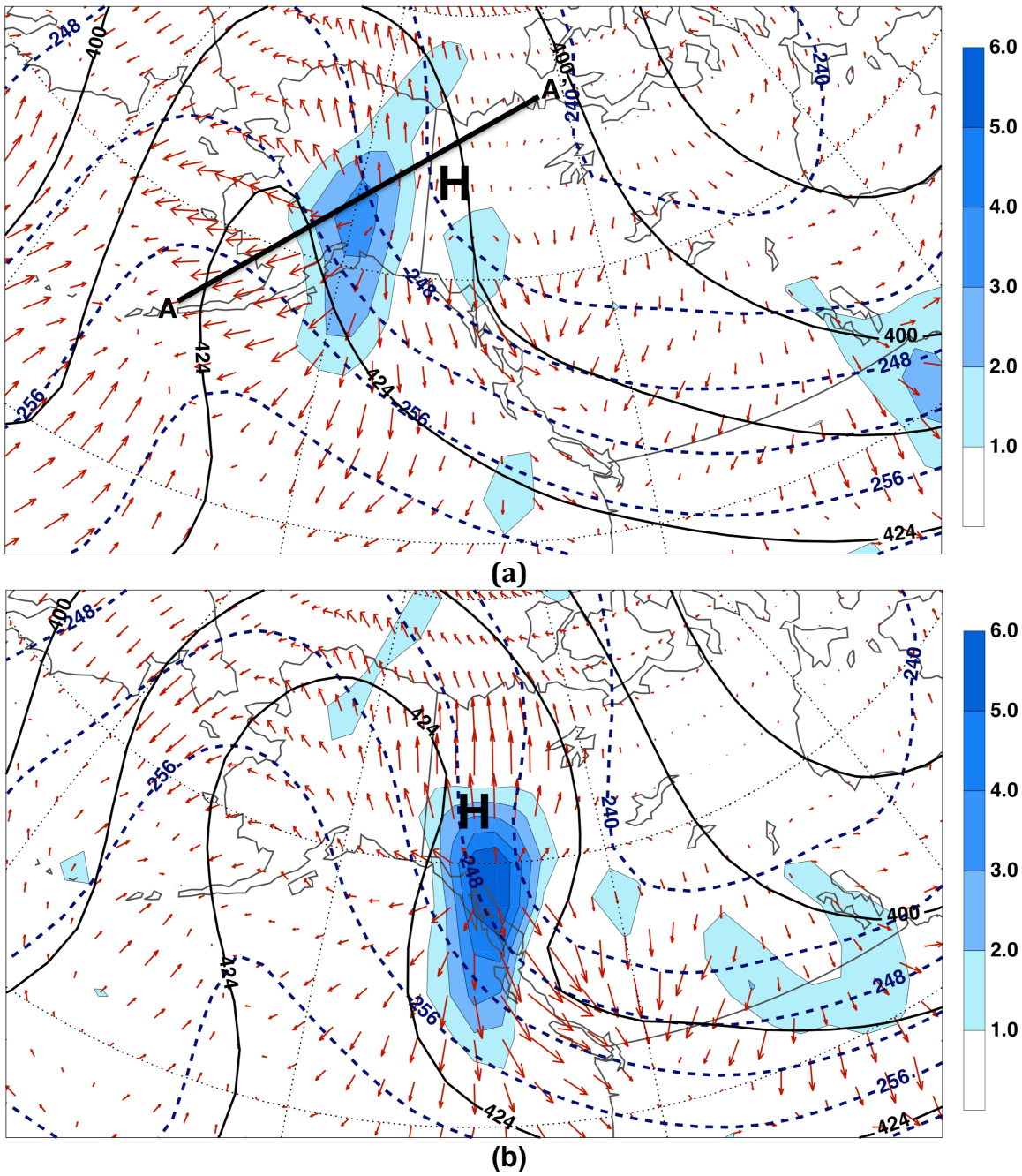

FIG. 8. 500–700 hPa column-averaged **Q**-vectors and **Q**-vector divergence (positive values shaded every 1.0 X 10^{-12} Pa m^{-2} s^{-1}), 500–700 hPa layer mean heights (solid contours, dam), and temperature (dashed, K) at (a) $t = -1$ day and (b) $t = 0$ for the Alaskan composite. A bold 'H' denotes the location of the surface anticyclone center.

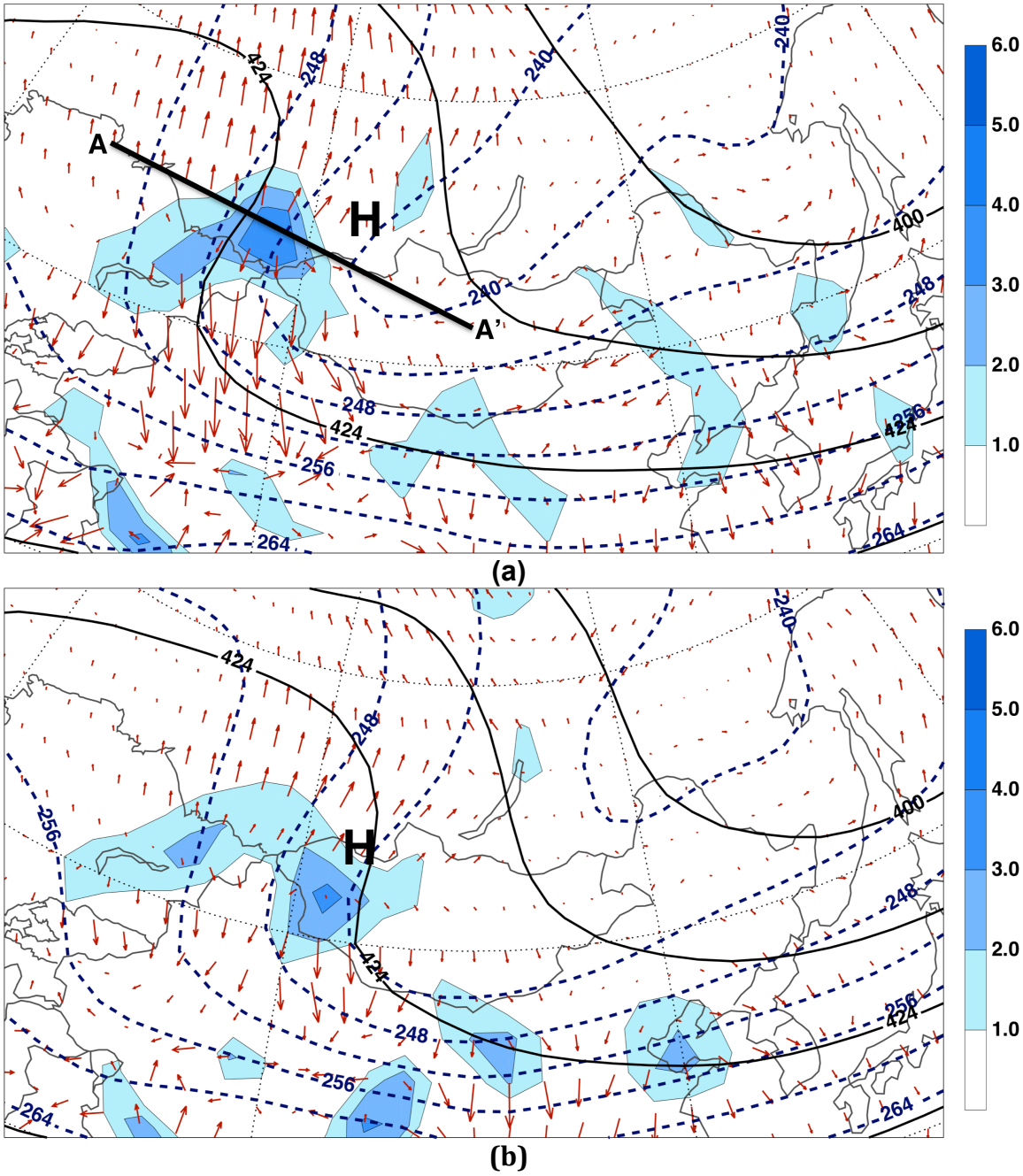

FIG. 9. As in FIG. 8, except for the Siberian composite.

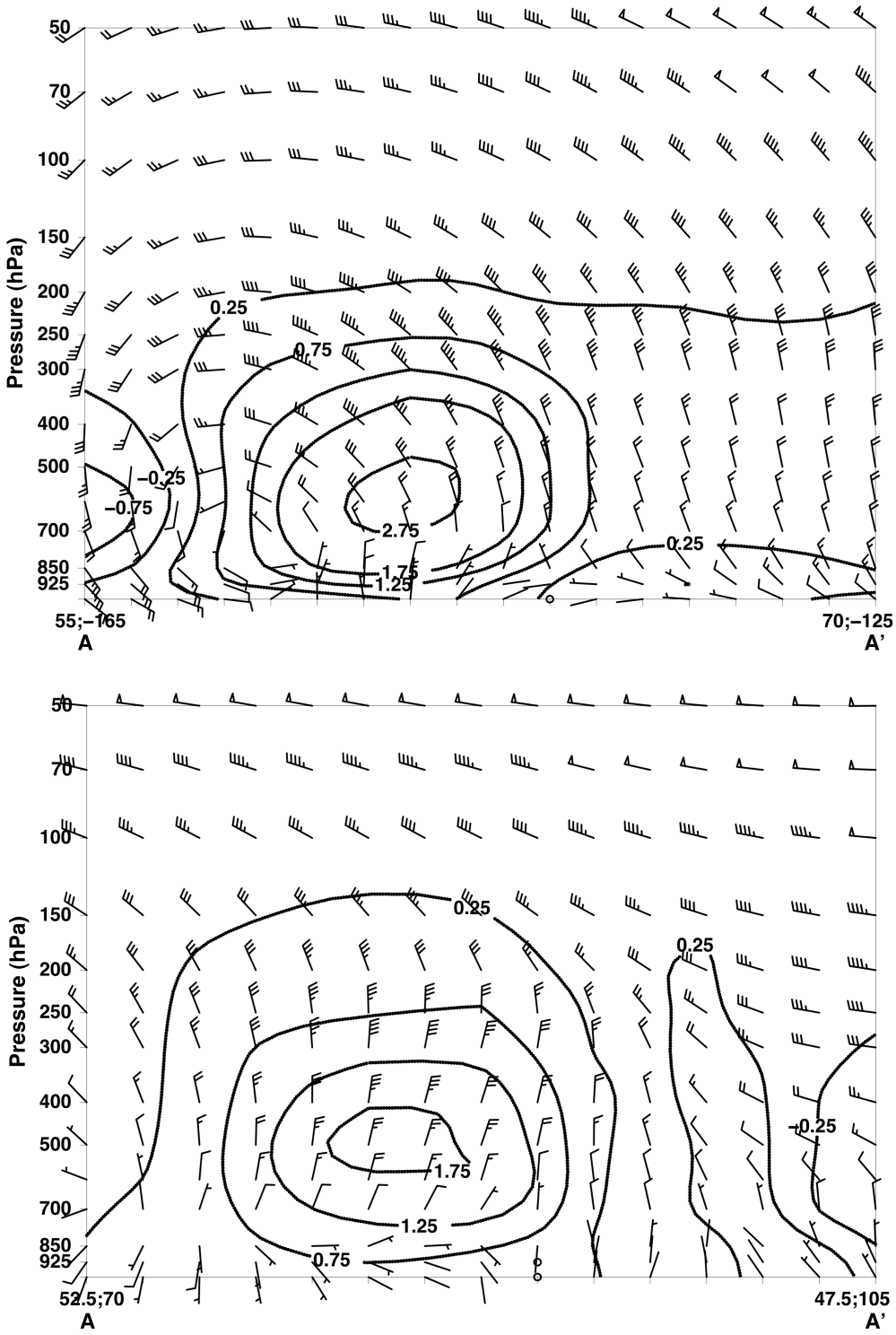

FIG. 10. Vertical cross-sections of ω (thicker contours, X 10^{-3} hPa s^{-1}) and winds (m s^{-1}) at t = −1 day for the Alaskan composite (top) and Siberian composite (bottom).

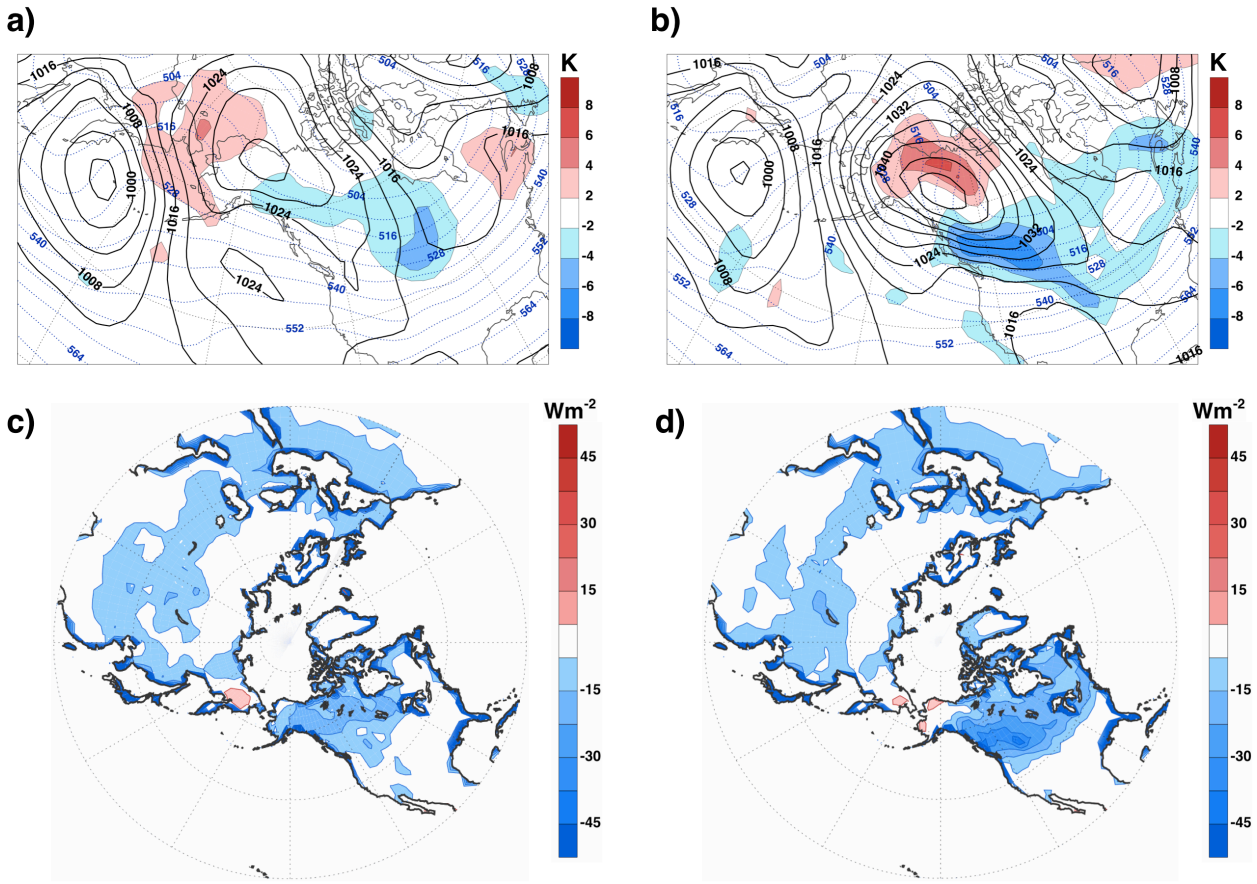

FIG. 11. SLP (solid contours, hPa) and 24-h difference of 925-hPa θ (shaded) centered at (a) $t = -2$ days and (b) $t = 0$ for the Alaskan composite. Net surface energy flux (W m^{-2}) at (c) $t = -2$ days and (d) $t = 0$.

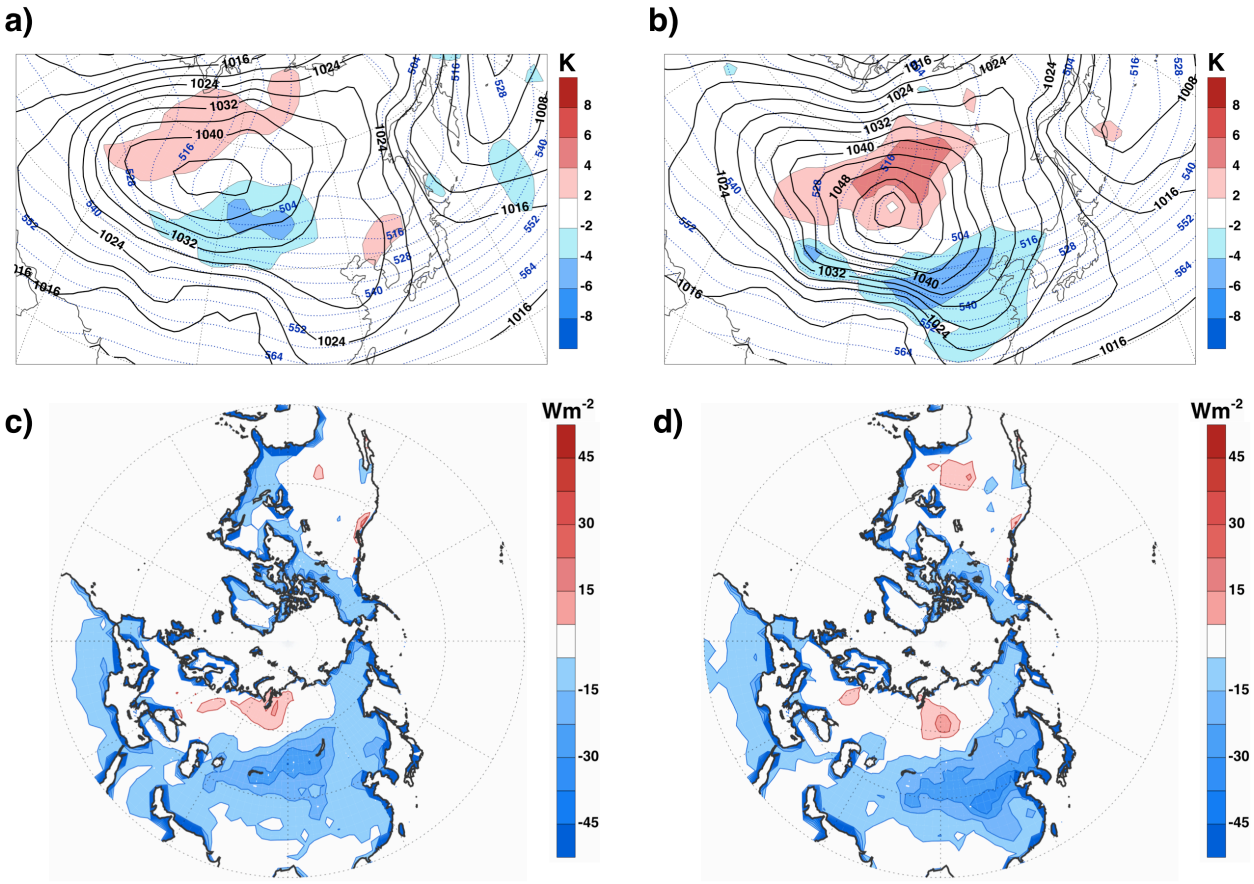

FIG. 12. As in FIG. 11, except for the Siberian composite.